

MR Insertable Brain PET Using Tileable GAPD Arrays

Key Jo Hong, Yong Choi, Jin Ho Jung, Jihoon Kang, Wei Hu, Hyun Keong Lim, Yoonsuk Huh, Sangsu Kim, Ji Woong Jung, Kyu Bom Kim, Myung Sung Song and Hyun-wook Park

Abstract—The aim of this study is to develop a MR compatible PET that is insertable to MRI and allows simultaneous PET and MR imaging of human brain. The brain PET having 72 detector modules arranged in a ring of 330 mm diameter was constructed and mounted in a 3-T MRI. Each PET module composed of 4×4 matrix of $3 \text{ mm} \times 3 \text{ mm} \times 20 \text{ mm}$ LYSO crystals coupled to a tileable 4×4 array Geiger-mode avalanche photodiode (GAPD) and designed to locate between RF and gradient coils. GAPD output charge signals were transferred to preamplifiers using flat cable of 3 m long, and then sent to position decoder circuit (PDC) identifying digital address and generating an analog pulse of the one interacted channel from preamplifier signals. The PDC outputs were fed into FPGA-embedded DAQ boards. The analog signal was digitized, and arrival time and energy of the signal were calculated and stored. LYSO and GAPD were located inside MR bore and all electronics including preamplifiers were positioned outside MR bore to minimize signal interference between PET and MR. Simultaneous PET/MR images of a hot-rod and Hoffman brain phantom were acquired in a 3-T MRI using the MR compatible PET system. The rods down to a diameter of 3.5 mm were resolved in the hot-rod PET image. Activity distribution patterns between white and gray matter in Hoffman brain phantom were well imaged. No degradation of image quality of the hot-rod and Hoffman brain phantoms on the simultaneously acquired MR images obtained with standard sequences was observed. These results demonstrate that simultaneous acquisition of PET and MR images is feasible using the MR insertable PET developed in this study.

I. INTRODUCTION

RECENTLY, positron emission tomography (PET) has evolved into multi-modality imaging systems obtaining quantitative functional information with accurate anatomical detail [1]. PET combined with computed tomography (CT) has been widely utilized in clinical and preclinical studies. As a subsequent advancement, a combination of PET and magnetic resonance imaging (MRI) has been proposed, not only because of the absence of ionizing radiation from MRI but also for its excellent soft-tissue contrast and its capability to perform

Manuscript received November 18, 2010. This study was supported by a grant of the Converging Research Center Program through the National Research Foundation of Korea (NRF) funded by the Ministry of Education, Science and Technology (2009-0081935), and by a grant of the Technology Innovation Program funded by, the Ministry of Knowledge Economy (10030029), Republic of Korea.

Key Jo Hong, Yong Choi, Jin Ho Jung, Jihoon Kang, Wei Hu, Hyun Keong Lim, Yoonsuk Huh, Sangsu Kim, Ji Woong Jung and Kyu Bom Kim are with the Department of Electronic Engineering, Sogang University, 1 Shinsu-Dong, Mapo-Gu, Seoul, 121-742, Republic of Korea (telephone: +82-2-705-8910, e-mail: ychoi@sogang.ac.kr, ychoi.image@gmail.com).

Myung Sung Song and Hyun-wook Park are with fMRI Laboratory N23, Department of Electrical Engineering, Korea Advanced Institute of Science and Technology, 373-1, Guseong-dong, Yuseong-gu, Daejeon, 305-701, Republic of Korea.

diffusion imaging, magnetic resonance spectroscopy (MRS) and functional MRI (fMRI) [2-4]. Thus, current developments on PET detector technology are focusing on the combination of PET and MRI to obtain simultaneous images from both modalities [5, 6].

The aim of this study is to develop a MR compatible PET using the GAPD that is insertable to MRI and allows simultaneous PET and MR imaging of human brain.

II. MATERIALS AND METHODS

A. PET detector module

Each PET detector module consisted of the 4×4 array LYSO (Sinoceramics, China) crystal and GAPD (SensL, Ireland). [7]. The LYSO array consisted of $3 \text{ mm} \times 3 \text{ mm} \times 20 \text{ mm}$ crystal pixels. The GAPD consisted of $3 \text{ mm} \times 3 \text{ mm}$ pixels and they arranged with a pitch of 3.3 mm. The GAPD has 3,640 micro-cells of $35 \mu\text{m} \times 35 \mu\text{m}$ size per individual GAPD pixel. Each crystal coupled one to one with an individual pixel of the GAPD without optical-coupling material. PET charge signals generated in the GAPD array were transmitted to the preamplifier using 300 cm flexible flat cable [8].

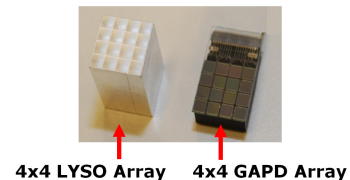


Fig. 1. 4×4 matrix LYSO crystals and a 4×4 array GAPD used to construct PET detector module.

B. Analog signal processing

The gain of preamplifier was 1000 times. The preamplifier board has a 16 channel output signals and has a digital bias controller for the GAPD bias voltage shown in Fig. 2 (left). The measured rise time, fall time and amplitude were 30 ns, 170 ns and 250 mV, respectively.

The position decoder circuit (PDC) decoded address and analog pulse of the interacted channel among the 64 preamplifier output signals shown in Fig. 2 (right) [9]. The channel reduction rate was 64 to 1.

C. Digital signal processing

The readouts of 18 analog signals and 126 bit digital signals were performed and processed by 14-bit free-running ADCs with 100 MHz sampling rate [10]. The digitized signals were then processed using a field programmable gate array (FPGA) board implemented to calculate the energy and timing information for a detected gamma ray.

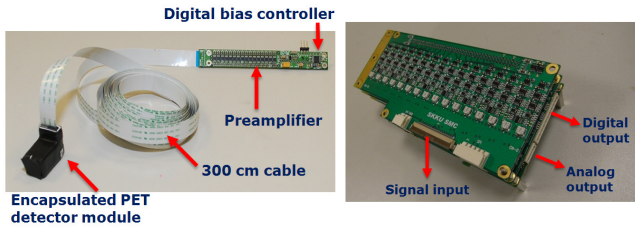


Fig. 2. PET detector module and preamplifier connected using flexible flat cable of 300 cm long (left) and photograph of the fabricated position decoder circuit board (right).

After the signal processing, the PET events with energy, arrival time and interacted position information were stored in list mode format data.

D. Brain PET system design

As shown in Fig. 3, The full ring PET scanner has 18 detector blocks arranged in a ring of 330 mm diameter with an axial field-of-view (FOV) of 12.9 mm. Each detector blocks consisted of 4 PET detector modules, 4 preamplifiers and 1 position decoder circuit. PET charge signals generated from the photosensor were transmitted through the long cable to the preamplifier circuits. Total 1,152 electrical channels of the PET scanner were amplified and processed using preamplifier, position decoder circuit and data acquisition units.

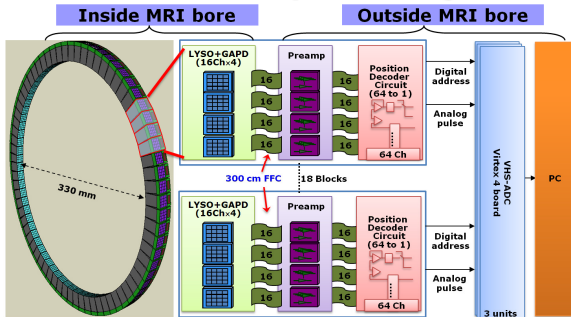


Fig.3. Brain PET system consisting of PET detectors, analog and digital electronics.

E. PET-MRI integration

The PET gantry was positioned inside the tunnel of a 3-Tesla Human MRI (ISOL Technology, Korea). A RF head coil of birdcage type was installed inside PET gantry used to transmit and receive the MRI data. The FOV of the PET-MRI is 12.9 mm in the axial direction, limited by the PET detector, and 250 mm in the transaxial direction, limited by the diameter of the RF coil. PET gantry including LYSO and GAPD array were located inside MR bore.

All electronics including preamplifiers were located outside MR bore to minimize the signal interference between MR and PET, as shown in Fig. 4. PET Gantry was shielded with gold plated mesh type fabric conductor. 300 cm cable was shielded with aluminum sheet.

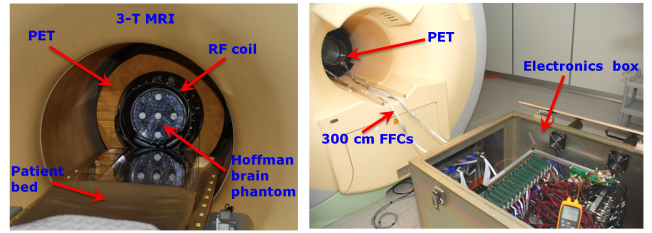


Fig. 4. Frontal (left) and rear (right) view of the PET gantry, with the RF coil placed inside 3-T MRI.

F. PET performance evaluations

Energy resolution, timing resolution and sensitivity were measured using a small point source of 3.7 MBq ^{18}F -FDG in a volume of 0.5 μL inside the tip of a small capillary tube [3]. The point source was located at the center of the PET scanner's FOV. PET data were acquired for 10 minutes with 350-650 keV energy threshold and a coincidence time window of 20 ns.

Spatial resolution was measured using ten 50 mm long glass capillary tubes with an inner diameter of 0.6 mm. The capillary was filled with approximately 0.5 MBq of ^{18}F -FDG line sources and positioned at different source-to-center distances (-8 cm, -6 cm, -4 cm, -2 cm, 0, 2 cm, 4 cm, 6 cm, 8 cm and 10 cm).

G. Phantom imaging

To demonstrate the feasibility of PET imaging using the brain PET system outside the magnet, PET data of a 3D Hoffman brain phantom (Data Spectrum Corporation, USA) were acquired for 100 min. The phantom was filled with 18.5 MBq of ^{18}F -FDG. The phantom image was reconstructed using a 2D filtered back projection (FBP).

A hot-rod and 3D Hoffman brain phantom was used to acquire simultaneous PET and MR images in the 3T MRI scanner using the MR compatible PET system. The phantoms were filled with 18.5 MBq of ^{18}F -FDG.

PET data of the hot-rod phantom were acquired simultaneously while MR imaging was performed using a T2-weighted gradient-echo sequence and a T1-weighted spin-echo sequence for 4 minutes. The phantom images were reconstructed using a 2D ordered subsets expectation maximization algorithm with 8 iterations and 8 subsets.

PET data of the 3D Hoffman brain phantom were acquired for 30 minutes with the PET insert outside the MRI and when installed inside the MRI while running T1-weighted spin-echo sequence. The phantom images were reconstructed using a 2D FBP. PET and MR images were analyzed by plotting a profile through the transverse slices crossing center FOV [3]. The obtained profiles were compared to measurements taken with the PET insert inside and outside the magnet.

For all phantom images, normalization and random correction were applied to improve image quality.

III. RESULTS

A. Basic performance of PET system

In measurements data acquired using the PET detector modules, the average energy resolution was 18.2% in the 64 channels using one PDC circuit. The 511 keV photopeak variation in the energy spectra was 8%.

Radial resolutions of reconstructed point source images acquired using the brain PET system ranged from 3.1 mm to 6.6 mm. The energy resolution, timing resolution and sensitivity were 20.8%, 4.2 ns and 0.3 %, respectively.

B. 3D Hoffman brain phantom imaging

Activity distribution patterns of 3D Hoffman brain phantoms were successfully acquired, as illustrated in Fig. 5. Activity distribution pattern between white and gray matter in Hoffman Brain phantom was well imaged.

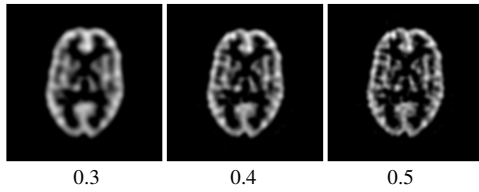


Fig. 5. Tomographic images of 3D Hoffman brain phantom acquired using the brain PET. The PET images were reconstructed by 2D FBP in a cut-off frequency ranged from 0.3 to 0.5

C. Simultaneous PET-MR phantom imaging

Fig. 6 shows simultaneously acquired PET, MRI and fused images of a hot-rod phantom while running MRI gradient echo and spin echo. The MR images showed no obvious distortion in the presence of PET insert when using standard MR pulse sequences. In PET image, the rods down to a diameter of 3.5 mm were resolved.

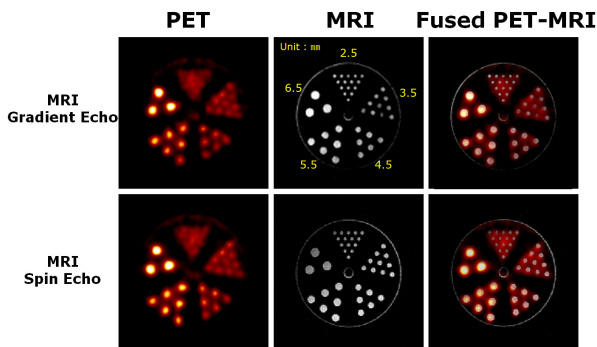


Fig. 6. PET (left), MRI (center) and fused images (right) of a hot-rod phantom acquired with MRI gradient echo (top) and spin echo (bottom).

Fig. 7 shows simultaneously acquired PET-MR images with MRI spin echo sequence. The activity distribution pattern between white and gray matter was well imaged for PET. MR image without noticeable artifacts and distortions was also acquired.

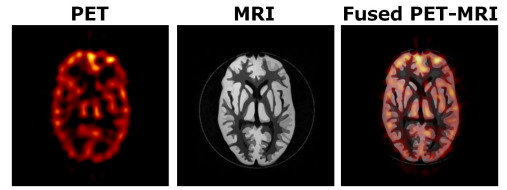


Fig. 7. PET (left), MRI (center) and fused images (right) of a 3D Hoffman brain phantom acquired with MRI spin echo sequence.

The quality of the simultaneously acquired PET-MR images were comparable to that of separately acquired PET and MR images, as shown in Fig. 8. There was little variation in the profiles of center FOV due to phantom refilling and repositioning.

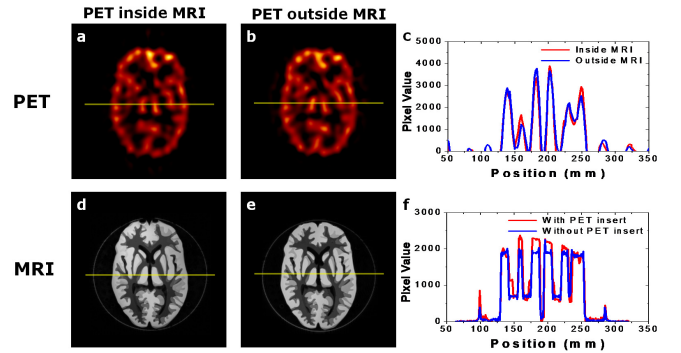


Fig. 8. PET images of a 3D Hoffman brain phantom acquired with the PET system operated inside the MRI system during a simultaneous MRI scan (a) and outside the MRI (b). MR images of a 3D Hoffman brain phantom taken with the PET insert installed and while acquired PET data (d) and in comparison MR images of the 3D Hoffman brain phantom acquired without the PET insert (e). The profiles drawn through the PET images (c) and the MR images (f).

IV. SUMMARY AND CONCLUSION

MR-compatible brain PET was designed and fabricated using newly developed GAPD-based PET detectors, charge signal transmission method using 300 cm cable, accurate PDC with high multiplexing ratio and digital signal processing with FPGA based ADC boards. PET images of the developed prototype PET were successfully acquired when MR images were simultaneously acquired using standard MRI sequences. MR images were acquired in the presence of the PET insert with standard pulse sequences without noticeable image artifacts and distortions. These results demonstrate that simultaneous acquisition of PET and MR image is feasible using the MR insertable PET developed in this study.

REFERENCES

- [1] D. W. Townsend, J. P. Carney, J. T. Yap, and N. C. Hall, "PET/CT today and tomorrow," *J. Nucl. Med.*, vol. 45 Suppl 1, pp. 4S-14S, Jan 2004.
- [2] P. Marzola, F. Osculati, and A. Sbarbati, "High field MRI in preclinical research," *Eur. J. Radiol.*, vol. 48, pp. 165-70, Nov 2003.

- [3] M. S. Judenhofer, H. F. Wehrl, D. F. Newport, C. Catana, S. B. Siegel, M. Becker, A. Thielscher, M. Kneilling, M. P. Lichy, M. Eichner, K. Klingel, G. Reischl, S. Widmaier, M. Rocken, R. E. Nutt, H. J. Machulla, K. Uludag, S. R. Cherry, C. D. Claussen, and B. J. Pichler, "Simultaneous PET-MRI: a new approach for functional and morphological imaging," *Nature Med.*, vol. 14, pp. 459-65, Apr 2008.
- [4] B. J. Pichler, H. F. Wehrl, A. Kolb, and M. S. Judenhofer, "Positron Emission Tomography/Magnetic Resonance Imaging: The Next Generation of Multimodality Imaging?," *Seminars in nuclear medicine*, vol. 38, pp. 199-208, 2008.
- [5] M. S. Judenhofer, C. Catana, B. K. Swann, S. B. Siegel, W. I. Jung, R. E. Nutt, S. R. Cherry, C. D. Claussen, and B. J. Pichler, "PET/MR Images Acquired with a Compact MR-compatible PET Detector in a 7-T Magnet," *Radiology*, vol. 244, pp. 807-814, 2007.
- [6] R. R. Raylman, S. Majewski, S. S. Velan, S. Lemieux, B. Kross, V. Popov, M. F. Smith, and A. G. Weisenberger, "Simultaneous acquisition of magnetic resonance spectroscopy (MRS) data and positron emission tomography (PET) images with a prototype MR-compatible, small animal PET imager," *J. Magn. Reson.*, vol. 186, pp. 305-10, Jun 2007.
- [7] K. J. Hong, Y. Choi, J. H. Kang, W. Hu, J. H. Jung, B. J. Min, H. K. Lim, S. H. Shin, Y. S. Huh, Y. H. Chung, P. Hughes, and C. Jackson, "Development of PET using 4 x 4 array of large size Geiger-mode avalanche photodiode," in *Nuclear Science Symposium Conference Record (NSS/MIC), 2009 IEEE*, 2009, pp. 3032-3037.
- [8] J. Kang, Y. Choi, K. J. Hong, J. H. Jung, W. Hu, Y. S. Huh, H. Lim, and B.-T. Kim, "A feasibility study of photosensor charge signal transmission to preamplifier using long cable for development of hybrid PET-MRI," *Med. Phys.*, vol. 37, pp. 5655-5664, 2010.
- [9] J. H. Jung, Y. Choi, K. J. Hong, W. Hu, J. H. Kang, B. J. Min, S. H. Shin, H. K. Lim, Y. S. Huh, and E. J. Kim, "Development of a position decoder circuit for PET consisting of GAPD arrays," *Nucl. Instrum. Meth. Phys. Res. Sec. A-Accelerators, Spectrometers, Detectors, and Associated equipment*, vol. 621, pp. 310-315, Sep 2010.
- [10] W. Hu, Y. Choi, K. J. Hong, J. Kang, J. H. Jung, Y. S. Huh, H. K. Lim, S. S. Kim, B. J. Min, and B.-T. Kim, "A simple and improved digital timing method for positron emission tomography," *Nucl. Instrum. Meth. Phys. Res. Sec. A-Accelerators, Spectrometers, Detectors, and Associated equipment*, vol. 622, pp. 219-224, 2010.